



Terahertz wafer-scale mobility mapping of graphene on insulating substrates without a gate

Buron, Jonas Due; Mackenzie, David M. A.; Petersen, Dirch Hjorth; Pesquera, Amaia; Centeno, Alba; Bøggild, Peter; Zurutuza, Amaia; Jepsen, Peter Uhd

Published in:
Optics Express

Link to article, DOI:
[10.1364/oe.23.030721](https://doi.org/10.1364/oe.23.030721)

Publication date:
2015

Document Version
Publisher's PDF, also known as Version of record

[Link back to DTU Orbit](#)

Citation (APA):
Buron, J. D., Mackenzie, D. M. A., Petersen, D. H., Pesquera, A., Centeno, A., Bøggild, P., Zurutuza, A., & Jepsen, P. U. (2015). Terahertz wafer-scale mobility mapping of graphene on insulating substrates without a gate. *Optics Express*, 23(24), 30721-30729. <https://doi.org/10.1364/oe.23.030721>

General rights

Copyright and moral rights for the publications made accessible in the public portal are retained by the authors and/or other copyright owners and it is a condition of accessing publications that users recognise and abide by the legal requirements associated with these rights.

- Users may download and print one copy of any publication from the public portal for the purpose of private study or research.
- You may not further distribute the material or use it for any profit-making activity or commercial gain
- You may freely distribute the URL identifying the publication in the public portal

If you believe that this document breaches copyright please contact us providing details, and we will remove access to the work immediately and investigate your claim.

Terahertz wafer-scale mobility mapping of graphene on insulating substrates without a gate

Jonas D. Buron,^{1,4} David M. A. Mackenzie,^{1,4} Dirch. H. Petersen,^{1,4} Amaia Pesquera,² Alba Centeno,² Peter Bøggild,^{1,4} Amaia Zurutuza,² and Peter U. Jepsen^{3,*}

¹DTU Nanotech - Department of Micro- and Nanotechnology, Technical University of Denmark, DK-2800 Kongens Lyngby, Denmark

²Graphenea S.A., Avenida de Tolosa, 76, 20018 - Donostia/San Sebastián, Spain

³DTU Fotonik - Department of Photonics Engineering, Technical University of Denmark, DK-2800 Kongens Lyngby, Denmark

⁴DTU Center for Nanostructured Graphene (CNG), DTU Nanotech - Department of Micro- and Nanotechnology, Technical University of Denmark, Denmark

*puje@fotonik.dtu.dk

Abstract: We demonstrate wafer-scale, non-contact mapping of essential carrier transport parameters, carrier mobility (μ_{drift}), carrier density (N_s), DC sheet conductance (σ_{dc}), and carrier scattering time (τ_{sc}) in CVD graphene, using spatially resolved terahertz time-domain conductance spectroscopy. σ_{dc} and τ_{sc} are directly extracted from Drude model fits to terahertz conductance spectra obtained in each pixel of $10 \times 10 \text{ cm}^2$ maps with a $400 \text{ }\mu\text{m}$ step size. σ_{dc} - and τ_{sc} -maps are translated into μ_{drift} and N_s maps through Boltzmann transport theory for graphene charge carriers and these parameters are directly compared to van der Pauw device measurements on the same wafer. The technique is compatible with all substrate materials that exhibit a reasonably low absorption coefficient for terahertz radiation. This includes many materials used for transferring CVD graphene in production facilities as well as in envisioned products, such as polymer films, glass substrates, cloth, or paper substrates.

©2015 Optical Society of America

OCIS codes: (120.4290) Nondestructive testing; (160.4236) Nanomaterials; (300.6250) Spectroscopy, condensed matter; (300.6495) Spectroscopy, terahertz; (310.3840) Materials and process characterization; (310.6870) Thin films, other properties.

References and links

1. F. Pizzocchero, B. S. Jessen, P. R. Whelan, N. Kotesha, S. Lee, J. D. Buron, I. Petrushina, M. B. Larsen, P. Greenwood, W. J. Cha, K. Teo, P. U. Jepsen, J. Hone, P. Bøggild, and T. J. Booth, "Non-destructive electrochemical graphene transfer from reusable thin-film catalysts," *Carbon* **85**, 397–405 (2015).
2. L. Tao, J. Lee, M. Holt, H. Chou, S. J. McDonnell, D. A. Ferrer, M. G. Babenco, R. M. Wallace, S. K. Banerjee, R. S. Ruoff, and D. Akinwande, "Uniform wafer-scale chemical vapor deposition of graphene on evaporated Cu (111) film with quality comparable to exfoliated monolayer," *J. Phys. Chem. C* **116**(45), 24068–24074 (2012).
3. J.-H. Lee, E. K. Lee, W.-J. Joo, Y. Jang, B.-S. Kim, J. Y. Lim, S.-H. Choi, S. J. Ahn, J. R. Ahn, M.-H. Park, C.-W. Yang, B. L. Choi, S.-W. Hwang, and D. Whang, "Wafer-scale growth of single-crystal monolayer graphene on reusable hydrogen-terminated germanium," *Science* **344**(6181), 286–289 (2014).
4. S. Rahimi, L. Tao, S. F. Chowdhury, S. Park, A. Jouvray, S. Buttress, N. Rupasinghe, K. Teo, and D. Akinwande, "Toward 300 mm wafer-scalable high-performance polycrystalline chemical vapor deposited graphene transistors," *ACS Nano* **8**(10), 10471–10479 (2014).
5. V. L. Nguyen, B. G. Shin, D. L. Duong, S. T. Kim, D. Perello, Y. J. Lim, Q. H. Yuan, F. Ding, H. Y. Jeong, H. S. Shin, S. M. Lee, S. H. Chae, Q. A. Vu, S. H. Lee, and Y. H. Lee, "Seamless stitching of graphene domains on polished copper (111) foil," *Adv. Mater.* **27**(8), 1376–1382 (2015).
6. T. Ma, W. Ren, Z. Liu, L. Huang, L.-P. Ma, X. Ma, Z. Zhang, L.-M. Peng, and H.-M. Cheng, "Repeated growth-etching-regrowth for large-area defect-free single-crystal graphene by chemical vapor deposition," *ACS Nano* **8**(12), 12806–12813 (2014).
7. S. Bae, H. Kim, Y. Lee, X. Xu, J.-S. Park, Y. Zheng, J. Balakrishnan, T. Lei, H. R. Kim, Y. I. Song, Y.-J. Kim, K. S. Kim, B. Özyilmaz, J.-H. Ahn, B. H. Hong, and S. Iijima, "Roll-to-roll production of 30-inch graphene films for transparent electrodes," *Nat. Nanotechnol.* **5**(8), 574–578 (2010).
8. K. S. Kim, Y. Zhao, H. Jang, S. Y. Lee, J. M. Kim, K. S. Kim, J.-H. Ahn, P. Kim, J.-Y. Choi, and B. H. Hong,

- “Large-scale pattern growth of graphene films for stretchable transparent electrodes,” *Nature* **457**(7230), 706–710 (2009).
9. Aixtron, Personal communication.
 10. J. Horng, C.-F. Chen, B. Geng, C. Girit, Y. Zhang, Z. Hao, H. A. Bechtel, M. Martin, A. Zettl, M. F. Crommie, Y. R. Shen, and F. Wang, “Drude conductivity of Dirac fermions in graphene,” *Phys. Rev. B* **83**(16), 165113 (2011).
 11. M. J. Paul, J. L. Tomaino, J. W. Kevek, T. DeBorde, Z. J. Thompson, E. D. Minot, and Y.-S. Lee, “Terahertz imaging of inhomogeneous electrodynamics in single-layer graphene embedded in dielectrics,” *Appl. Phys. Lett.* **101**(9), 091109 (2012).
 12. C. Cervetti, E. Heintze, B. Gorshunov, E. Zhukova, S. Lobanov, A. Hoyer, M. Burghard, K. Kern, M. Dressel, and L. Bogani, “Sub-terahertz frequency-domain spectroscopy reveals single-grain mobility and scatter influence of large-area graphene,” *Adv. Mater.* **27**(16), 2635–2641 (2015).
 13. J. D. Buron, D. H. Petersen, P. Bøggild, D. G. Cooke, M. Hilke, J. Sun, E. Whiteway, P. F. Nielsen, O. Hansen, A. Yurgens, and P. U. Jepsen, “Graphene conductance uniformity mapping,” *Nano Lett.* **12**(10), 5074–5081 (2012).
 14. J. Tomaino, A. Jameson, M. Paul, J. Kevek, A. van der Zande, R. Barton, H. Choi, P. McEuen, E. Minot, and Y.-S. Lee, “High-contrast imaging of graphene via time-domain terahertz spectroscopy,” *J. Infrared Millim. Terahertz Waves* **33**(8), 839–845 (2012).
 15. L. Ren, Q. Zhang, J. Yao, Z. Sun, R. Kaneko, Z. Yan, S. Nanot, Z. Jin, I. Kawayama, M. Tonouchi, J. M. Tour, and J. Kono, “Terahertz and infrared spectroscopy of gated large-area graphene,” *Nano Lett.* **12**(7), 3711–3715 (2012).
 16. J. D. Buron, F. Pizzocchero, P. U. Jepsen, D. H. Petersen, J. M. Caridad, B. S. Jessen, T. J. Booth, and P. Bøggild, “Graphene mobility mapping,” *Sci. Rep.* **5**, 12305 (2015).
 17. P. U. Jepsen, D. G. Cooke, and M. Koch, “Terahertz spectroscopy and imaging – Modern techniques and applications,” *Laser Photonics Rev.* **5**(1), 124–166 (2011).
 18. J. D. Buron, F. Pizzocchero, B. S. Jessen, T. J. Booth, P. F. Nielsen, O. Hansen, M. Hilke, E. Whiteway, P. U. Jepsen, P. Bøggild, and D. H. Petersen, “Electrically continuous graphene from single crystal copper verified by terahertz conductance spectroscopy and micro four-point probe,” *Nano Lett.* **14**(11), 6348–6355 (2014).
 19. D. M. A. Mackenzie, J. D. Buron, P. R. Whelan, B. S. Jessen, A. Silajdžić, A. Pesquera, A. Centeno, A. Zurutuza, P. Bøggild, and D. H. Petersen, “Fabrication of CVD graphene-based devices via laser ablation for wafer-scale characterization,” *2D Mater.* **2**(4), 045003 (2015).
 20. L. J. Van Der Pauw, “A method of measuring the resistivity and Hall coefficient on lamellae of arbitrary shape,” *Philips Tech. Rev.* **20**, 220–224 (1958).
 21. D. H. Petersen, O. Hansen, R. Lin, and P. F. Nielsen, “Micro-four-point probe Hall effect measurement method,” *J. Appl. Phys.* **104**(1), 013710 (2008).
 22. M. R. Lotz, M. Boll, O. Hansen, D. Kjær, P. Bøggild, and D. H. Petersen, “Revealing origin of quasi-one dimensional current transport in defect rich two dimensional materials,” *Appl. Phys. Lett.* **105**, 053115 (2014).
 23. M. Boll, M. R. Lotz, O. Hansen, F. Wang, D. Kjær, P. Bøggild, and D. H. Petersen, “Sensitivity analysis explains quasi-one-dimensional current transport in two-dimensional materials,” *Phys. Rev. B* **90**(24), 245432 (2014).
 24. G. Inawali, Y. Rao, H. Yan, and T. F. Heinz, “Observation of a transient decrease in terahertz conductivity of single-layer graphene induced by ultrafast optical excitation,” *Nano Lett.* **13**(2), 524–530 (2013).
 25. I. Maeng, S. Lim, S. J. Chae, Y. H. Lee, H. Choi, and J.-H. Son, “Gate-controlled nonlinear conductivity of Dirac fermion in graphene field-effect transistors measured by terahertz time-domain spectroscopy,” *Nano Lett.* **12**(2), 551–555 (2012).
 26. J. M. Dawlaty, S. Shivaraman, J. Strait, P. George, M. Chandrashekar, F. Rana, M. G. Spencer, D. Veksler, and Y. Chen, “Measurement of the optical absorption spectra of epitaxial graphene from terahertz to visible,” *Appl. Phys. Lett.* **93**(13), 131905 (2008).
 27. H. Choi, F. Borondics, D. A. Siegel, S. Y. Zhou, M. C. Martin, A. Lanzara, and R. A. Kaindl, “Broadband electromagnetic response and ultrafast dynamics of few-layer epitaxial graphene,” *Appl. Phys. Lett.* **94**(17), 172102 (2009).
 28. Z. Q. Li, E. A. Henriksen, Z. Jiang, Z. Hao, M. C. Martin, P. Kim, H. L. Stormer, and D. N. Basov, “Dirac charge dynamics in graphene by infrared spectroscopy,” *Nat. Phys.* **4**(7), 532–535 (2008).
 29. A. H. Castro Neto, F. Guinea, N. M. R. Peres, K. S. Novoselov, and A. K. Geim, “The electronic properties of graphene,” *Rev. Mod. Phys.* **81**(1), 109–162 (2009).
 30. E. H. Hwang, S. Adam, and S. D. Sarma, “Carrier transport in two-dimensional graphene layers,” *Phys. Rev. Lett.* **98**(18), 186806 (2007).
 31. T. Ando, “Screening effect and impurity scattering in monolayer graphene,” *J. Phys. Soc. Jpn.* **75**(7), 074716 (2006).
 32. K. Nomura and A. H. MacDonald, “Quantum transport of massless Dirac fermions,” *Phys. Rev. Lett.* **98**(7), 076602 (2007).
 33. D. Vasileska, https://nanohub.org/resources/1578/download/ddmodel_mobility_word.pdf.
 34. G. Ng, D. Vasileska, and D. K. Schroder, “Calculation of the electron Hall mobility and Hall scattering factor in 6H-SiC,” *J. Appl. Phys.* **106**(5), 053719 (2009).
 35. G. Rutsch, R. P. Devaty, W. J. Choyke, D. W. Langer, and L. B. Rowland, “Measurement of the Hall scattering

- factor in 4H and 6H SiC epilayers from 40 to 290 K and in magnetic fields up to 9 T,” J. Appl. Phys. **84**(4), 2062–2064 (1998).
36. J. Náhlík, I. Kašpárková, and P. Fitl, “Study of quantitative influence of sample defects on measurements of resistivity of thin films using van der Pauw method,” Measurement **44**(10), 1968–1979 (2011).
 37. L. A. Ponomarenko, R. Yang, T. M. Mohiuddin, M. I. Katsnelson, K. S. Novoselov, S. V. Morozov, A. A. Zhukov, F. Schedin, E. W. Hill, and A. K. Geim, “Effect of a high- κ environment on charge carrier mobility in graphene,” Phys. Rev. Lett. **102**(20), 206603 (2009).
 38. R. S. Popovic, *Hall Effect Devices*, 2nd ed. (Institute of Physics, 2003).

1. Introduction

Graphene synthesis technology is rapidly approaching a commercially viable level, where continuous graphene films of high structural integrity are routinely produced on wafer-scale [1–6] or even m² scale [7,8], with projected throughput of order 10⁵ m²/year for CVD production tools [9]. Even so, no viable means for assessing consistency in electronic properties across these length scales or area production rates are currently offered by the prevailing electronic characterization methods, typically based on field-effect or Hall mobility measurements in lithographically defined devices. Over the past five years, several demonstrations of non-contact techniques for characterization of graphene electrical properties have been reported [10–15]. Most techniques, however, gauge the graphene conductance rather than the other primary parameters of interest, which are the carrier mobility, μ , and sheet carrier density, N_s . Recently we presented spatial mapping of field-effect mobility and carrier density of large-area chemical vapor deposition (CVD) graphene by non-contact, back-gated terahertz time-domain conductance spectroscopy (THz-TDS) [16]. While potentially very useful in the development and optimization phase of 2D material synthesis and transfer, the approach requires deposition of the graphene film on a gate-stack substrate, and is thus not directly applicable to the many applications and production scenarios involving graphene films on insulating and flexible substrates. These include some of the most lucrative technologies such as graphene photovoltaics, displays, and flexible electronics, where *in-line* characterization and quality-control require the THz-TDS analysis to be carried out on the native substrate. The present work is a step in that direction, presenting a novel non-contact approach for rapid spatial mapping of carrier drift mobility (μ_{drift}) and carrier density of four inch graphene wafers. The technique, which is based on direct measurement of the terahertz carrier dynamics by time domain spectroscopy [13,17,18], does not require the use of carrier density control by a back gate, and is compatible with a broad range of common graphene substrates, including various polymers, glasses, and insulating metal oxides. In addition to providing a means of non-destructive and rapid measurement of graphene drift mobility and carrier density in scenarios without a gate or external magnetic field, the method is significantly faster than previously demonstrated methods [16], and provides additional information on transport dynamics such as carrier scattering rate and mean free path.

2. Experimental setup & methods

2.1 Terahertz time-domain spectroscopy

We employ a THz time-domain spectrometer based on photoconductive antennas [13], to map the electromagnetic response from 0.25 to 1.2 THz of charge carriers in an approximately 95 mm wide CVD graphene film residing on a 4-inch wafer substrate. As shown in Fig. 1(a), the substrate consists of 525 μm high resistivity silicon, 50 nm p + -doped polycrystalline silicon, and 165 nm low pressure chemical vapor deposited stoichiometric silicon nitride (Si₃N₄). The THz-transparent back gate, consisting of the p + doped polysilicon layer [16], was not needed in this study, however, and was left at floating potential. An approximately 10 mm wide area near one edge of the silicon wafer is kept free from graphene in the transfer process. As indicated in Fig. 1(a), the sample is raster scanned in the focal plane of the THz beam, which is focused to a diffraction limited spot with a frequency-

dependent full-width-at-half-maximum (FWHM) ranging from approximately 1.0 mm at 0.25 THz to 0.3 mm above 1.0 THz. The entire 4-inch wafer is raster-mapped in steps of 400 μm , where the transmitted THz transient is recorded in each pixel of the map. Figure 1(b) shows an example of such a transmitted THz transient as well as a comparison to a THz transient transmitted through the non-graphene-covered area of the 4-inch sample. As described elsewhere [13,17], THz-TDS is particularly sensitive to free carrier absorption, and thus the fast Fourier transforms (FFT) of THz time-domain transients, $\tilde{E}_{ref}(\nu) = \text{fft}[E_{ref}(t)]$ and $\tilde{E}_{graphene}(\nu) = \text{fft}[E_{graphene}(t)]$, transmitted through silicon substrate and silicon substrate covered with graphene, respectively, can be related directly to the complex sheet conductance, $\tilde{\sigma}_s(\nu)$, of the graphene film at THz frequencies as:

$$\tilde{T}(\nu) = \frac{\tilde{E}_{graphene}(\nu)}{\tilde{E}_{ref}(\nu)} = \frac{1 + n_{sub}}{1 + n_{sub} + Z_0 \tilde{\sigma}_s(\nu)}. \quad (1)$$

Sheet conductance spectra, such as the ones shown in Fig. 1(c), are extracted in each pixel of the mapped area using Eq. (1).

2.2 Van der Pauw device fabrication & Hall measurements

As shown in Fig. 1(d), Ti/Au contacts were deposited onto the graphene film subsequent to THz-TDS analysis, by electron beam evaporation through an aluminum shadow mask. The graphene film was patterned by picosecond laser ablation into 5 mm wide square van der Pauw (vdP) devices, suitable for dual-configuration sheet conductance and Hall effect measurements to extract carrier mobility and carrier density [19]. Dual configuration measurements suppress geometrical errors in both sheet conductance [20] and Hall effect measurements [21] and allow the electrical continuity to be determined [13,18,22,23]. With a constant applied external magnetic field of $B_{ext} = 255 \text{ mT}$, the resistances R_A , R_B and R_C were measured in the three electrode configurations, defined from Fig. 1(e) as

$$R_A = \frac{I_{12}}{V_{34}}, R_A' = \frac{I_{21}}{V_{43}}, R_B = \frac{I_{24}}{V_{31}}, R_B' = \frac{I_{42}}{V_{13}}, R_C = \frac{I_{23}}{V_{41}}, R_C' = \frac{I_{32}}{V_{14}} \quad (2)$$

Sheet conductance $\sigma_s = 1/R_s$, Hall mobility μ_{Hall} , and Hall carrier density $N_{s,Hall}$, were obtained according to

$$\exp[-\pi R_A/R_s] + \exp[-\pi R_C/R_s] = 1, \quad (3)$$

$$R_{Hall} = (R_B - R_B')/2, \quad (4)$$

$$N_{s,Hall} = B_{ext} / (q R_{Hall}), \quad (5)$$

$$\mu_{Hall} = 1 / (e N_{s,Hall} R_s), \quad (6)$$

where q is the electronic charge.

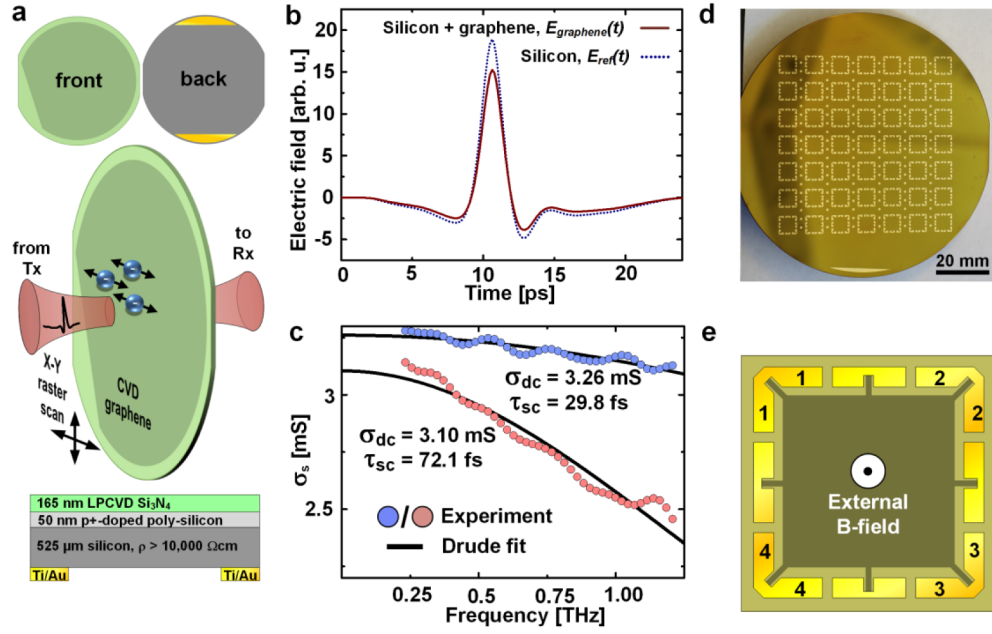


Fig. 1. (a) The sample is a 100 mm wide CVD graphene film on a 4-inch layered wafer substrate, consisting of 525 μm high resistivity silicon, 50 nm p + -doped poly-Si, and 165 nm LPCVD Si₃N₄. An approximately 10 mm wide area near one edge of the silicon wafer is kept free from graphene in the transfer process. The sample is raster scanned in the focal plane of the THz beam to form spatially resolved maps. (b) Examples of THz time-domain transients recorded after transmission through the sample (c) σ_s spectra (real part) extracted from time-domain measurements at two different graphene locations, showing different τ_{sc} . (d) vdP devices are formed after THz-TDS mapping by shadow mask deposition of Ti/Au contacts, and patterning of the graphene film by picosecond laser to form (e) 5 mm wide, square devices. μ_{Hall} and $N_{s,Hall}$ is determined from measurements of resistances in the A-, B-, and C-configurations in a constantly applied externally magnetic field of 255 mT.

Crucially, the chosen method allows for definition of vdP devices, without affecting the electronic properties of the active area of the graphene film by introduction of photolithographic or electron beam lithographic resist, solvents, or other chemicals.

3. Results and discussion

Consistent with previous observations in THz-TDS [18,24,25] and FTIR [10,15,26–28] studies of graphene, we find the conductance dynamics to be well described by the Drude model, given by

$$\tilde{\sigma}_s(\omega) = \frac{\sigma_{s,dc}}{1 - i\omega\tau}, \quad (7)$$

where σ_{DC} is the sheet conductance at DC, τ_{sc} is the carrier momentum relaxation time, and ω is the angular frequency. By fitting the Drude model to the real part of the conductance spectrum in each pixel of the recorded map, σ_{DC} and τ_{sc} can be mapped, as shown in Fig. 2. The imaginary part of the measured sheet conductance was not used in the fitting routine, because of large systematic errors due to variations across the sample in the substrate thickness. In principle, inclusion of the imaginary part of the extracted conductance could increase the reliability of the fit. However, even the slightest variations of substrate thickness across the wafer results in a significant systematic error in the extraction of the imaginary part of the conductance, which is not the case for the real part. While this systematic error can to

some extent be quantified and corrected [16], in the present case, a fit to the real part of the conductance alone results in robust estimates of the DC conductance and scattering time.

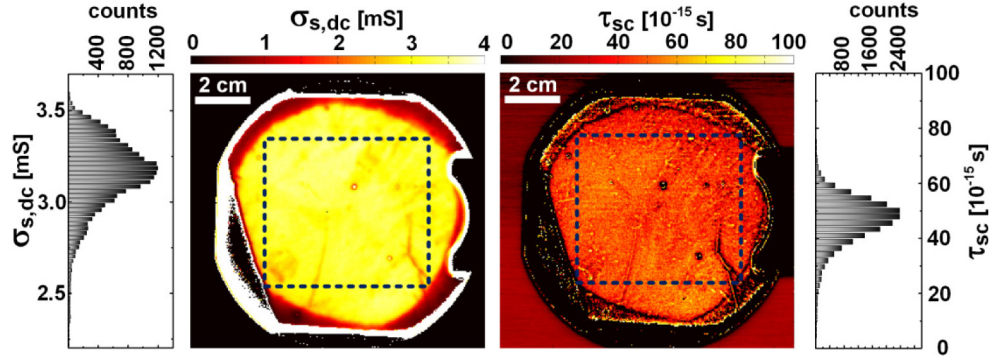


Fig. 2. Spatial maps of σ_{dc} and τ_{sc} obtained by raster-scanned THz-TDS analysis. Histograms show distributions of σ_{dc} and τ_{sc} within the dashed squares marked on the maps.

In the limit of $k_B T \ll E_F$, the dc conductance can be expressed as [10,24,29–32]

$$\sigma_{s,dc} = q^2 v_F \tau_{sc} \sqrt{N_s} / (\hbar \sqrt{\pi}), \quad (8)$$

where v_F is the Fermi velocity taken to be 10^6 m/s [29]. Thus, carrier drift mobility and carrier density can be evaluated across the 4-inch wafer, as shown in Fig. 3(a), from measurements of $\sigma_{s,dc}$ and τ_{sc} , by using the relations

$$N_s = \frac{\pi \hbar^2}{q^4 v_F^2} \left(\frac{\sigma_{s,dc}}{\tau_{sc}} \right)^2, \quad (9)$$

$$\mu_{drift} = \frac{\sigma_{s,dc}}{e N_s} = \frac{q^3 v_F^2}{\pi \hbar^2} \frac{\tau_{sc}^2}{\sigma_{s,dc}} = \frac{q v_F}{\sqrt{\pi \hbar}} \frac{\tau_{sc}}{\sqrt{N_s}}$$

It should be noted that this analysis does not provide any information on the dependence of τ_{sc} and thus μ_{drift} on N_s , because the THz-TDS measurements are carried out at constant N_s . For transport in graphene films limited by long-range carrier scattering on charged impurities, however, the scattering rate is expected to scale as $\tau_{sc} \propto \sqrt{N_s}$, yielding a drift mobility that is independent of carrier density.

Figure 3(b) shows histograms of drift mobilities and carrier densities normalized to their average values, constructed from measured values within the dashed rectangles in Fig. 2(a). The measured drift mobility follows a Gaussian distribution with an average value of 845 cm^2/Vs , and a standard deviation of 244 cm^2/Vs , corresponding to a relative standard deviation of 0.28. Meanwhile, the carrier density displays a distribution skewed towards higher concentration, which is more accurately described by an extreme value distribution. The graphene film exhibits a high unintentional doping level, with an average carrier density of $2.25 \times 10^{13} \text{ cm}^{-2}$. The standard deviation of measured carrier densities is $0.56 \times 10^{13} \text{ cm}^{-2}$, resulting in a relative standard deviation of 0.25. This is slightly lower, but of the order of the standard deviation found for μ_{drift} .

While the determination from THz-TDS carrier dynamics provides the drift carrier mobility and carrier density, as defined in the Drude model, conventional device measurements of carrier mobility and density typically provide either the Hall or field-effect mobility and density. These may differ from the parameters as defined in Drude theory, due to several effects. Firstly, it is known from theory [33,34] and analysis [35] of 3D

semiconductor materials that Hall mobility and drift mobility can in some cases differ fundamentally by a factor known as the Hall scattering factor. Secondly, geometrical effects, related to e.g. inhomogeneities of the graphene film can strongly affect the measured device transport properties measurements, so that the inferred material properties deviate significantly from the intrinsic properties [13,18].

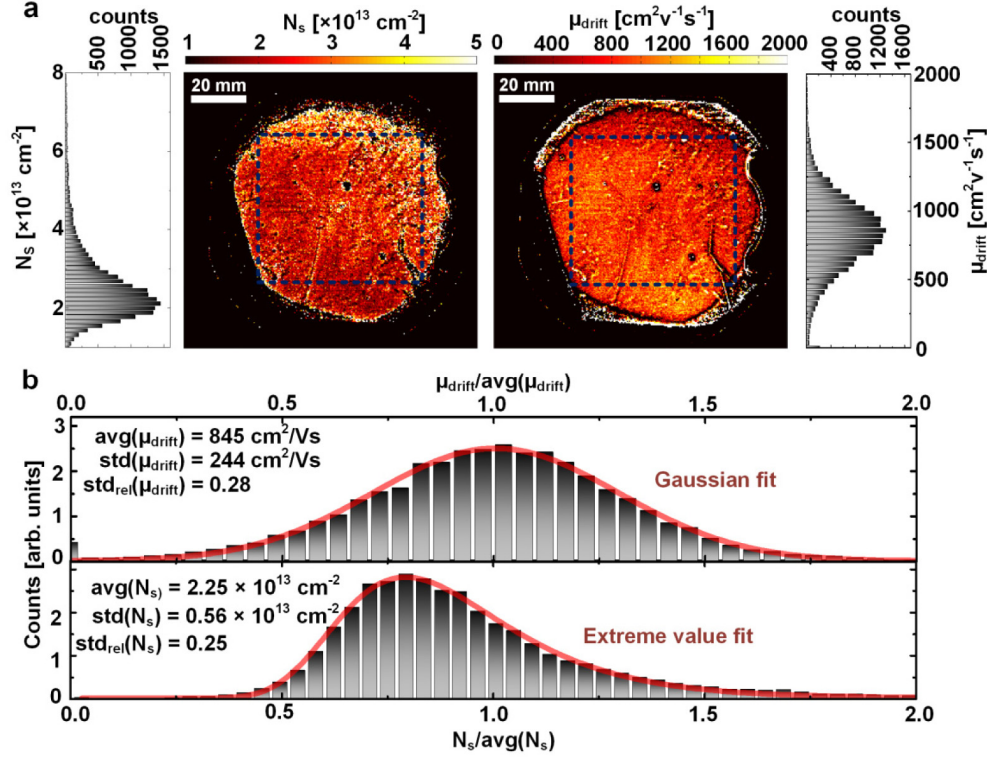


Fig. 3. (a) Maps of N_s and μ_{drift} derived from σ_{dc} and τ_{sc} -maps in Fig. 2. Distributions of N_s and μ_{drift} within the dashed squares marked on the maps. (b) Distribution of N_s and μ_{drift} relative to their average values.

To investigate how conventional device measurements of carrier mobility and carrier density relate to the THz-TDS measurements of μ_{drift} and N_s , van der Pauw structures (shown in Fig. 1(c)) suitable for dual-configuration Hall measurements were fabricated in the same graphene film shown in Figs. 2 and 3. Measurements of $\sigma_{s,\text{dc}}$, μ_{Hall} , and $N_{s,\text{Hall}}$ in 47 individual $5 \times 5 \text{ mm}^2$ devices are compared to the average values of $\sigma_{s,\text{dc}}$, μ_{drift} , and N_s , obtained by THz-TDS inside the active device regions, in Figs. 4(a), 4(b), and 4(c), respectively. As can be observed in Fig. 4, the spread in $\sigma_{s,\text{dc}}$, μ_{Hall} , and $N_{s,\text{Hall}}$ measured in vdP structures is quite large compared to the significantly smaller spread in $\sigma_{s,\text{dc}}$, μ_{drift} , and N_s measured by THz-TDS. As we have shown in previous correlation studies [13,18], however, defects on the scale of the device dimensions can greatly affect the electronic parameters determined by vdP device measurements [22,23,36], while the THz-TDS outcome is much less affected, due to its much smaller characteristic carrier transport length (tens to hundreds of nm). The ratio of resistances R_A/R_C , measured in two different electrode configurations provides a unique signature of the presence of such extended defects in the devices, where a device with a continuous active region, free from such extended defects will fulfil the criterion of electrical continuity [18], which in this case is $R_A/R_C \approx 1$.

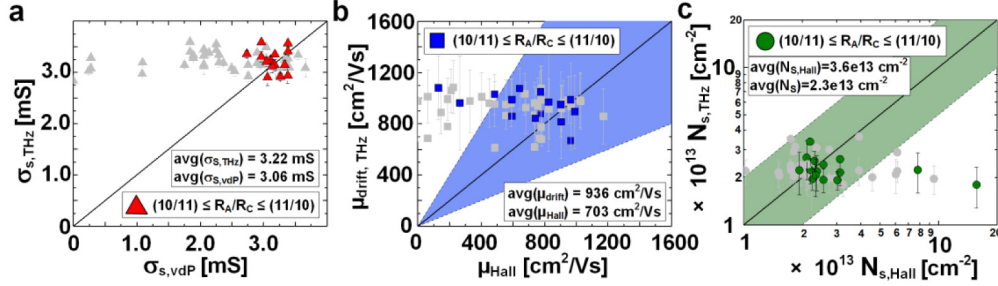


Fig. 4. Comparison of transport properties measured by THz-TDS and dual-configuration Hall effect method (a) $\sigma_{s,THz}$ vs $\sigma_{s,vdP}$ (b) μ_{drift} vs. μ_{Hall} (c) N_s . The full diagonal lines represent 1:1 correlation, while shaded areas represent 2:1 correlation or better. Error bars represent the standard deviation of the 36 THz-TDS pixels per device. Colored markers correspond to areas where the vdP dual configuration measurements indicate highly homogeneous / continuous conductance.

When only including dual configuration vdP device measurements with a relatively narrow acceptance window in terms of electrical continuity, i.e. $0.91 \leq R_A / R_C \leq 1.1$ (colored markers), the spread is significantly decreased, and the correlation between vdP measurements and THz-TDS measurements dramatically improved. We thus observe a strong 1:1 correlation of sheet conductance measurements between vdP and THz-TDS, and a correlation of μ_{Hall} to μ_{drift} , and $N_{s,Hall}$ to N_s , which except for two outliers, are within a factor two. The presented THz-TDS based mapping technique thus accurately provides the intrinsic sheet conductance of CVD graphene films, as well as carrier drift mobility and carrier density to within at least a factor of 2. It should be noted that the observed discrepancy between μ_{drift} and μ_{Hall} , as well as $N_{s,THz}$ and $N_{s,Hall}$ may arise from fundamental differences in the intrinsic material parameters, as reflected by a non-unity Hall scattering factor [35,37,38]. The observed correlation is however not strong enough to conclude on the significance of this effect.

The presented technique is compatible with all substrate materials that exhibit a reasonably low absorption coefficient for terahertz radiation. This includes many materials used for transferring CVD graphene in production facilities as well as in envisioned products, such as polymer films, glass substrates, cloth, or paper substrates. Such wide tolerances in terms of substrate properties is a consequence of μ_{drift} , N_s , τ_{sc} , and $\sigma_{s,dc}$ being directly determined from the terahertz conductance dynamics, eliminating the need for application of gate- or magnetic fields or even patterning of devices. We note that this opens up the prospect of quantitative, non-invasive mapping of the essential graphene performance indicators, $\sigma_{s,dc}$, μ_{drift} and N_s , during the polymer-assisted transfer step, which is integral to most production line scenarios. This type of integrated, in-line quality management will be increasingly important, as graphene production and applications leaves its present embryonic state to compete with existing material technologies. We anticipate that this capability can prove disruptive for the extent as well as nature of industrial CVD graphene characterization and standardization.

7. Conclusion

We address the challenge of rapid, non-contact, electronic characterization of carrier mobility and density of large-area graphene without the need for a back-gate, externally applied magnetic fields, patterning of devices, or contact deposition. Using mapped terahertz time-domain spectroscopy, we were able to extract the carrier mobility, carrier density, scattering time and DC sheet conductance across a 4-inch wafer sized CVD graphene film with 400 μm resolution. Direct comparison to measurements of sheet conductance, Hall mobility and Hall carrier density in mm-sized devices carved from the same CVD graphene film by laser-

ablation, show similar values, where $\overline{\sigma_{s,THz}}/\overline{\sigma_{s,vdp}} = 1.02 \pm 0.09$, $\overline{\mu_{drift,THz}}/\overline{\mu_{Hall}} = 1.33 \pm 0.50$, and $\overline{N_{s,THz}}/\overline{N_{s,Hall}} = 0.63 \pm 0.62$. We anticipate that our findings will pave the way for new standards pertaining electronic characterization of graphene in production scenarios, as our presented technique facilitates quantitative, non-invasive mapping of the essential graphene performance indicators, μ_{drift} and N_s , during the polymer-assisted transfer step which is integral to most production line scenarios.

Acknowledgments

We acknowledge financial support from the EC Graphene FET Flagship, contract no 604391, Center for Nanostructured Graphene (CNG), sponsored by the Danish National Research Foundation, Project DNRF58, and the Villum Foundation, project no. VKR023117.